Subsurface Evolution and Persistence of Marine Heatwaves in the Northeast Pacific

Hillary A. Scannell[1,1], Gregory C. Johnson[2,2], LuAnne Thompson[3,3], John M. Lyman[4,4], and Stephen C. Riser[3,3]

[1]School of Oceanography, University of Washington, Seattle, WA, USA
[2]Pacific Marine Environmental Laboratory, NOAA, Seattle, WA, USA
[3]School of Oceanography, University of Washington, Seattle, WA, USA.
[4]Pacific Marine Environmental Laboratory, NOAA, Seattle, WA, USA.

November 30, 2022

Abstract

The reappearance of a northeast Pacific marine heatwave (MHW) sounded alarms in late summer 2019 for a warming event on par with the 2013–2016 MHW known as The Blob. Despite these two events having similar magnitudes in surface warming, differences in seasonality and salinity distinguish their evolutions. We compare and contrast the ocean's role in the evolution and persistence of the 2013–2016 and 2019–2020 MHWs using mapped temperature and salinity data from Argo floats. An unusual near-surface freshwater anomaly in the Gulf of Alaska during 2019 increased the stability of the water column, preventing the MHW from penetrating as deeply as the 2013–2016 event. This freshwater anomaly likely contributed to the intensification of the MHW by increasing the near-surface buoyancy. The gradual buildup of subsurface heat content throughout 2020 in the region suggests the potential for persistent ecological impacts.

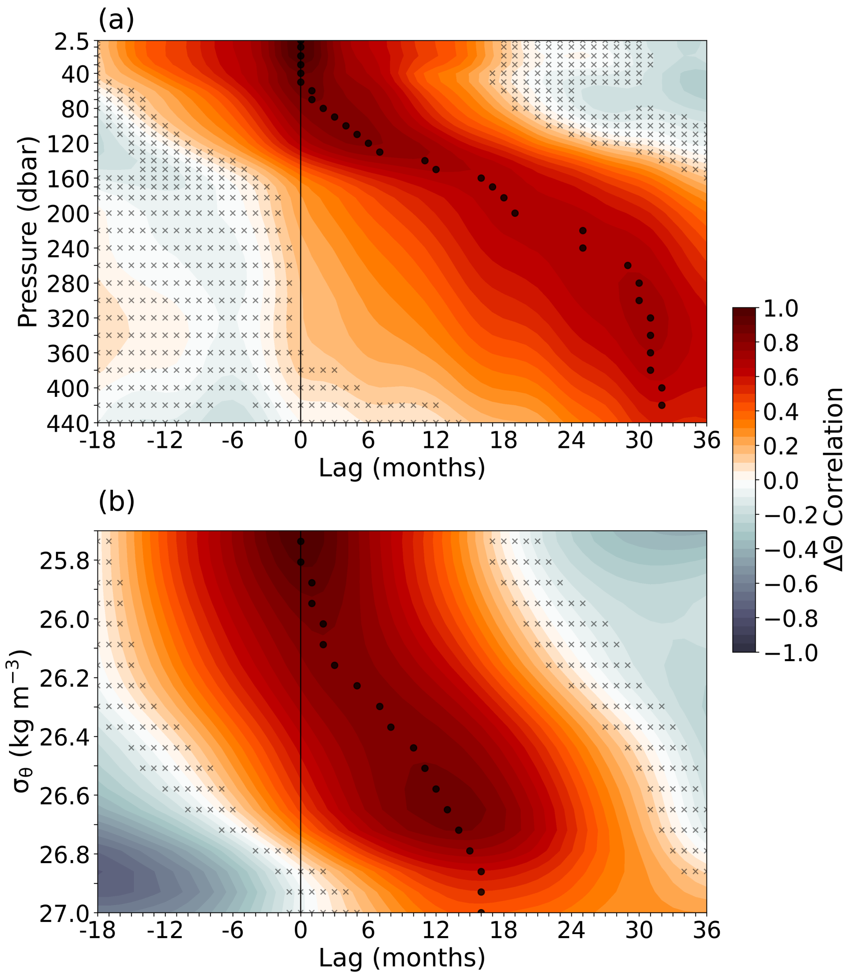
(a)
Pressure (dbar)
2.5
40
80
120
160
200
240
280
320
360
400
440
-18 -12 -6 0 6 12 18 24 30 36
Lag (months)
(b)
σθ (kg m−3)
25.8
26.0
26.2
26.4
26.6
26.8
27.0
-18 -12 -6 0 6 12 18 24 30 36
Lag (months)
ΔΘ Correlation
1.0 0.8 0.6 0.4 0.2 0.0 −0.2 −0.4 −0.6 −0.8 −1.0

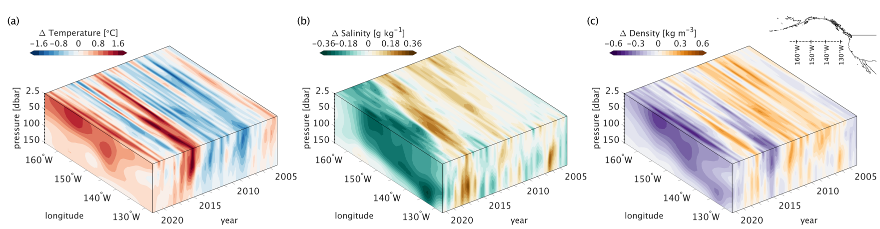
(a)
Δ Temperature [°C]
−1.6 −0.8 0 0.8 1.6
pressure [dbar]
2.5
50
100
150
160°W
150°W
140°W
130°W
longitude
2020
2015
2010
2005
year
(b)
Δ Salinity [g kg−1]
−0.36 −0.18 0 0.18 0.36
(c)
Δ Density [kg m−3]
−0.6 −0.3 0 0.3 0.6

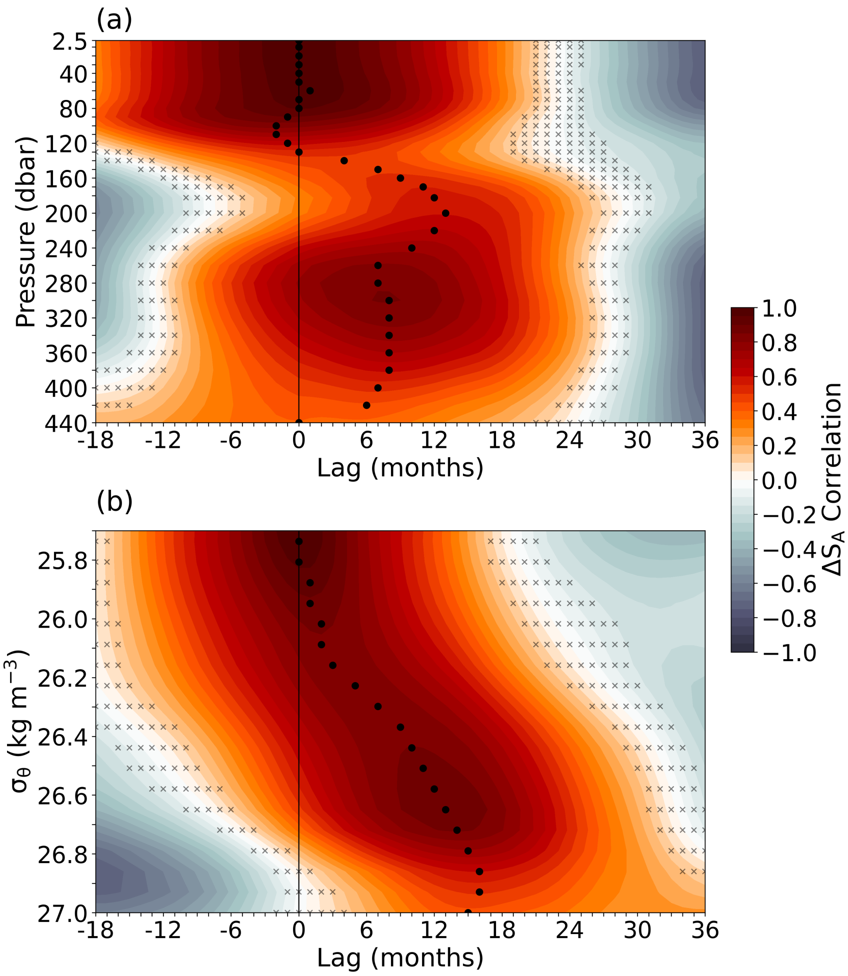
(a)
Pressure (dbar)
Lag (months)
(b)
σ_θ (kg m^{-3})
Lag (months)
ΔS_A Correlation

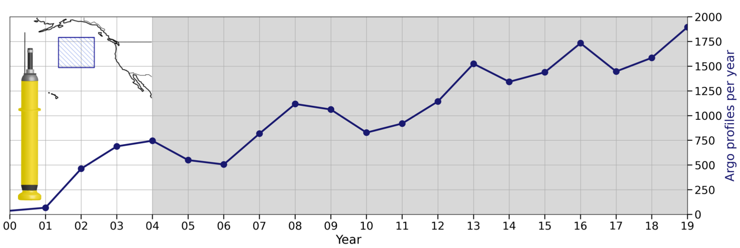
Year
Argo profiles per year

Subsurface Evolution and Persistence of Marine Heatwaves in the Northeast Pacific

H. A. Scannell[1], G. C. Johnson[2], L. Thompson[1], J. M. Lyman[2,3], S. C. Riser[1]

[1]School of Oceanography, University of Washington, Seattle, WA, USA.

[2]Pacific Marine Environmental Laboratory, NOAA, Seattle, WA, USA.

[3]Joint Institute for Marine and Atmospheric Research, University of Hawaii at Manoa, Honolulu, HI, USA.

Corresponding author: Hillary A. Scannell (scanh@uw.edu)

Key Points :

- Return of The Blob, with warming and freshening, hence more buoyancy.
- Summertime heatwaves, increase stratification, inhibit mixing.
- Wintertime mixing, warming penetrates the deep, provides memory.

Abstract

The reappearance of a northeast Pacific marine heatwave (MHW) sounded alarms in late summer 2019 for a warming event on par with the 2013–2016 MHW known as The Blob. Despite these two events having similar magnitudes in surface warming, differences in seasonality and salinity distinguish their evolutions. We compare and contrast the ocean's role in the evolution and persistence of the 2013–2016 and 2019–2020 MHWs using mapped temperature and salinity data from Argo floats. An unusual near-surface freshwater anomaly in the Gulf of Alaska during 2019 increased the stability of the water column, preventing the MHW from penetrating as deeply as the 2013–2016 event. This freshwater anomaly likely contributed to the intensification of the MHW by increasing the near-surface buoyancy. The gradual buildup of subsurface heat content throughout 2020 in the region suggests the potential for persistent ecological impacts.

Plain Language Summary

Surface marine heatwaves (MHWs) are periods of prolonged and extremely warm regional sea surface temperature that can negatively impact the health and productivity of marine ecosystems. Using surface and subsurface ocean observations, we compare and contrast two recent MHWs to show that salinity variations play an important role in the vertical distribution of temperature anomalies by changing the overall stability of the water column. During the 2019–2020 MHW, the near-surface waters in the Gulf of Alaska were fresher than normal, preventing warm sea surface temperatures from mixing as deeply into the subsurface as in the 2013–2016 MHW. The freshening in 2019 likely enhanced warming in the buoyant surface layer. As warmer temperatures gradually mix downward they can persist long after the surface MHW disappears, suggesting that the ocean can provide memory for long-lived MHWs. The subsurface persistence of MHWs has potential ramifications for long-lasting ecological impacts.

1 Introduction

Marine heatwaves (MHWs) have become distinguishable features of northeast (NE) Pacific Ocean temperature variability that disrupt the productivity of marine ecosystems and their services (Smale et al., 2019). These prolonged, discrete, and anomalously warm water events (Hobday et al., 2016) are most recognizable at the sea surface and are influenced by anthropogenic warming (Laufkötter, et al., 2020). The effects of long-term ocean warming have led to a near-doubling in the average annual count of MHW days globally since the early 20th Century (Oliver et al., 2018). Although MHWs have occurred throughout the global ocean, the NE Pacific has recently emerged as a hotspot for extremely persistent and large-scale events that are forced by anomalous air-sea heat flux driven by remote forcing from the tropics (Di Lorenzo and Mantua, 2016; Holbrook et al., 2019), in addition to long-term warming from anthropogenic greenhouse forcing (Laufkötter, et al., 2020). The most remarkable NE Pacific MHWs have occurred in 2013–2016 and 2019–2020, and are colloquially referred to as The Blob (Bond et al., 2015) and Blob2.0 (Amaya et al., 2020) respectively (Figure 1 and Figure S1).

The magnitude of sea surface temperature (SST) anomalies associated with MHWs depends critically on the seasonal evolution of the mixed-layer depth (MLD), which deepens in winter and shoals in summer. If winter mixed layer MHW anomalies are present in the early spring when the NE Pacific MLD shoals, they can become trapped in the subsurface during the summer through detrainment. These detrained temperature anomalies are then stored in the subsurface and can reemerge the following winter when the MLD deepens and re-entrains them (Alexander and Deser, 1995; Alexander et al, 1999; Alexander et al., 2001). Alternatively, in the presence of downward Ekman pumping from wind stress curl, for example in the North Pacific subtropical gyre, detrained anomalies can subduct, where they are further isolated from the mixed layer (Qiu and Huang, 1995). Here, we explore the role of detrainment and subduction in the sequestration of MHW anomalies into the permanent pycnocline where they can persist for years.

The evolution of the 2013–2016 NE Pacific MHW was complex and shaped by multiple drivers. Warm SST anomalies first appeared in the southern Gulf of Alaska centered on 40°N and 150°W and subsequently propagated towards the coast and south into the Southern California Current System near 25°N. In the Gulf of Alaska, lower rates of turbulent heat loss during the winter of 2013–2014 from the ocean to atmosphere and a reduction in wind-generated stirring allowed the winter mixed layer to remain unseasonably warm and shallow (Bond et al., 2015). The MWH moved to the south owing to local positive downward shortwave radiation anomalies and a positive SST-cloud feedback over the Southern California Current System that reinforced surface warming near the coast in 2014 (Zaba and Rudnick, 2016; Myers et al., 2018; Schmeisser et al., 2019). Below the mixed layer, anomalously warm and salty water was detrained to denser and deeper isopycnals, reaching depths of 140 m beginning in 2014 (Jackson et al., 2018). These subsurface anomalies lingered through at least 2018, long after the initial onset of atmospheric forcing in late 2013.

A similar situation played out during the summer of 2019 when a resurgence of Blob-like surface conditions intensified in the NE Pacific. Weakened surface wind speeds, driven by atmospheric teleconnections associated with SST anomalies in the Tropical Pacific, resulted in reduced evaporative heat loss from the ocean to atmosphere and limited wind-driven mixing, resulting in a MHW off the U.S. West Coast (Amaya et al., 2020). Increased shortwave radiation and a positive SST-cloud feedback helped to maintain the MHW over an exceptionally shallow summertime mixed layer (Amaya et al., 2020). Here, we show evidence for the role of salinity anomalies in increasing upper ocean stability, and describe the propagation and persistence of the 2019–2020 NE Pacific MHW in the subsurface.

In this study, we examine the connections between surface MHWs and the subsurface structure of temperature, salinity, and density by analyzing objectively mapped monthly Argo data in the NE Pacific, comparing and contrasting the 2013–2016 and 2019–2020 MHWs. We characterize the spatiotemporal evolution of anomalous subsurface conditions and their connection to mixed layer properties from January 2004 through June 2020, and we quantify the change in water mass properties and ocean heat content anomalies within and below the mixed layer. Understanding the subsurface evolution and persistence of MHWs gives insight into the potential predictability and reemergence of these events in the future, where a trend towards shallower summertime MLDs is expected to increase the likelihood and intensity of MHWs in the North Pacific (D.J. Amaya, personal communication, 2020). The persistence and potential reoccurrence of MHWs could result in long-lasting impacts on the health of marine ecosystems, especially in the subsurface where the effects of warming on marine life (i.e., thermal stress) can persist for years (Cavole et al., 2016).

2 Data

We analyze monthly mean SST maps from the Optimum Interpolation SST version 2 (OISSTv2) dataset on a 0.25° longitude by 0.25° latitude global grid from 1982 through present (Reynolds et al., 2002; 2007). These SST maps are generated from a blend of satellite (Advanced Very High Resolution Radiometer only), ship, buoy (both moored and drifting), and Argo float data. The satellite data are interpolated to fill gaps and are bias corrected with reference to buoys to account for platform differences. We use the OISSTv2 dataset as it incorporates *in situ* observations, offers complete global coverage, and spans almost 40 years.

We also analyze monthly mean fields from January 2004 through June 2020 from the updated Roemmich-Gilson Argo Climatology (Roemmich and Gilson, 2009; hereafter RG09) to examine the vertical structure of temperature, salinity, and density anomalies associated with MHWs. Argo is a global network of autonomous profiling floats that continuously measures the temperature and salinity of the upper 2,000 m of the ocean. The Argo program began in 1999 and now consists of over 3,800 active floats and more than 2 million hydrographic profiles reported thanks to a coordinated effort from dozens of countries worldwide (Jayne et al., 2017). Archived and near real-time float data are made publicly available (http://sio-argo.ucsd.edu/RG_Climatology.html) and are incorporated into monthly maps on a 1° longitude by 1° latitude grid beginning in January 2004 when the global array had at least 1,000 floats and first approached sparse global coverage (RG09). These maps are made in 58 pressure layers with the shallowest centered on 2.5 dbar and the deepest on 1,975 dbar, with finer resolution near the surface (e.g., spaced 10 dbar apart from 10 to 170 dbar). The 2.5 dbar monthly temperature anomalies in RG09 closely track the monthly OISSTv2 anomalies in the NE Pacific, capturing large scale spatial and temporal variability.

In addition to the mapped temperature and salinity vs. pressure fields from RG09, we also analyze 19,697 quality-controlled Argo profiles in the NE Pacific (35.5–51.5°N, 135.5–154.5°W; box in Figure 1) to compute the MLD from January 2004 through June 2020 using the density algorithm of Holte and Talley (2009). The sampling frequency from Argo in the NE Pacific (35.5–51.5°N, 135.5–154.5°W) steadily increases from the early 2000s, achieving over 1,000 profiles per year starting in 2012 (Figure S2). These profiles were downloaded from one of the two Argo Global Data Assembly Centers (https://nrlgodae1.nrlmry.navy.mil/argo/argo.html) in August 2020.

3 Analysis

We define MHWs locally when SST exceeds the monthly climatological 90th percentile for at least a month using monthly data from January 2004 through June 2020. Our definition for MHWs is similar to that proposed in Hobday et al. (2016) with modifications in the length of the climatological period and in the minimum event duration. Owing to the prominence and persistence of the 2013–2016 and 2019–2020 MHWs, our definition highlights the same large-scale features described in previous studies using daily data (e.g., Gentemann et al., 2017; Fewings and Brown, 2019).

Before analyzing the RG09 dataset, we fit temperature and salinity at each spatial point to the mean, trend, annual, and semiannual harmonics using least squares regression from January 2004 through June 2020. We then remove the mean, annual, and semi-annual harmonics (but not the trend) to generate anomalies. Following MHW conventions (e.g., Hobday et al., 2016), we choose to retain the warming trend in the analysis using a fixed climatology computed over the entire record. Furthermore, the trend would not be accurately estimated over such a short period and would be extremely biased by the 2013–2016 and 2019–2020 MHWs at one end of the time-series. Finally, detrending would effectively remove part of the strong MHW signal that we observe towards the latter end of the record. We therefore retain it. Next, we smooth the anomalies and the regression coefficients with a 5-month Hanning filter and then a 6° latitude x 6° longitude LOESS filter to reduce mesoscale signals that are retained in the RG09 maps. We then reconstruct the total smoothed *in-situ* temperature and practical salinity maps using the smoothed anomalies and smoothed model coefficients. We apply the thermodynamic equation of seawater (Intergovernmental Oceanographic Commission et al., 2010) to compute the absolute salinity (S_A) and conservative temperature (Θ) at each space and time grid point. Using S_A and Θ, we also compute the potential density anomaly (σ_θ) with reference to 0 dbar; expressed as a particular potential density minus 1000 kg m^{-3}. The potential density represents the density a fluid parcel would acquire if it were brought adiabatically to the sea surface, thus eliminating the density dependence on pressure. We also map the RG09 fields of S_A, Θ, and pressure (P) to a vertical density coordinate, σ_θ. We compute anomalies in S_A, Θ, and P in σ_θ coordinates, as well as S_A, Θ, and σ_θ in P coordinates, by removing the monthly means of these quantities across the entire 198-month time series at each spatial point and for each vertical coordinate system (σ_θ and P) to get the anomalies. We describe changes in S_A, Θ, and P on an isopycnal (25.4 kg m^{-3}) that may outcrop during winter. When isopycnals outcrop their properties are easily modified through air-sea interactions that may drive surface MHWs. Once isopycnals subduct below the mixed layer, their properties are only modified through mixing, which is usually less effective than direct air-sea heat and freshwater exchange.

We examine the ocean heat content anomaly (Q') within the mixed layer (10–90 dbar), thermocline (100–180 dbar), and just below the thermocline (200–280 dbar). These layers of equal thickness are chosen based on the vertical profiles of subsurface temperature in the NE Pacific (Figure 4b). They typify the surface, pycnocline, and interior ocean in the region, allowing for the distinction of the changes in Q' with depth. We define $Q' = \int \frac{1}{g} \cdot c_p \cdot \Theta' dp$, where $g = 9.8\ \mathrm{ms^{-2}}$ is the acceleration due to gravity, $c_p = 3991.8680\ \mathrm{J\ kg^{-1} K^{-1}}$ is the standard specific heat of seawater when using Θ, Θ' is the conservative temperature anomaly, and $\int dp$ is the integral over each of these three 80-dbar thick layers.

We apply the Holt and Talley (2009) density algorithm to 19,697 Argo float profiles in the NE Pacific (35.5–51.5°N, 135.5–154.5°W; box in Figure 1) to estimate monthly MLDs from January 2004 through June 2020. This method searches for the depth at which the density increases by 0.03 kg m^{-3} relative to a near-surface reference level.

We quantify the bulk stratification of the upper ocean using the Brunt-Väisälä frequency squared $N^2 = -\frac{g}{\rho}\frac{d\rho}{dz}$. Here, $\frac{d\rho}{dz}$ is the change in potential density with reference to 0 dbar between 2.5 and 200 dbar. Larger values of N^2 correspond to greater upper ocean stratification — a more stable water column. We compute anomalies in N^2, again with respect to monthly long-term means, to quantify the change in the stratification of the upper ocean due to MHW variations in both Θ and S_A.

To further examine the relationships among Θ, S_A, and σ_θ, we examine $\Theta - S_A$ diagrams with contours of constant density and spice to show changes in water-mass properties between different MHW years in the NE Pacific. $\Theta - S_A$ variations along isopycnals can be quantified by spice (Munk, 1981), where warm/salty anomalies are spicy and cool/fresh anomalies are minty. We compute spice following McDougall and Krzysik (2015) using a potential density with reference to 0 dbar. Isopycnal variations in spiciness can be used to describe MHW impacts on isopycnal water-mass properties in density units.

4 Results

Anomalies in $\Theta - S_A$ on isopycnals can be tracked following the surface evolution of SST anomalies during MHWs, and can either be warm/salty (spicy) or cool/fresh (minty), such that the density of that isopycnal does not change (Movie S1). The winter-intensified 2013–2016 MHW had spicy anomalies on 25.4 kg m^{-3}, which lagged the spatiotemporal evolution of SST anomalies within the MHW (Movie S1, hatching in Figure 1). For example, surface MHW conditions moved onshore by late 2014 and began to fade as early as 2015, whereas subsurface spice anomalies did not reach the coast until winter 2015 and persisted into 2016 (Movie S1). By comparison, summer $\Theta - S_A$ anomalies in 2019 lacked the advective nature of the 2013–2016 MHW, yet they were much more widespread. Minty anomalies on 25.4 kg m^{-3} encompassed nearly the entire Gulf of Alaska from late summer 2018 through summer 2020, while spicy anomalies lingered off the coast between Baja California and Hawai'i (Figure 1, Movie S1).

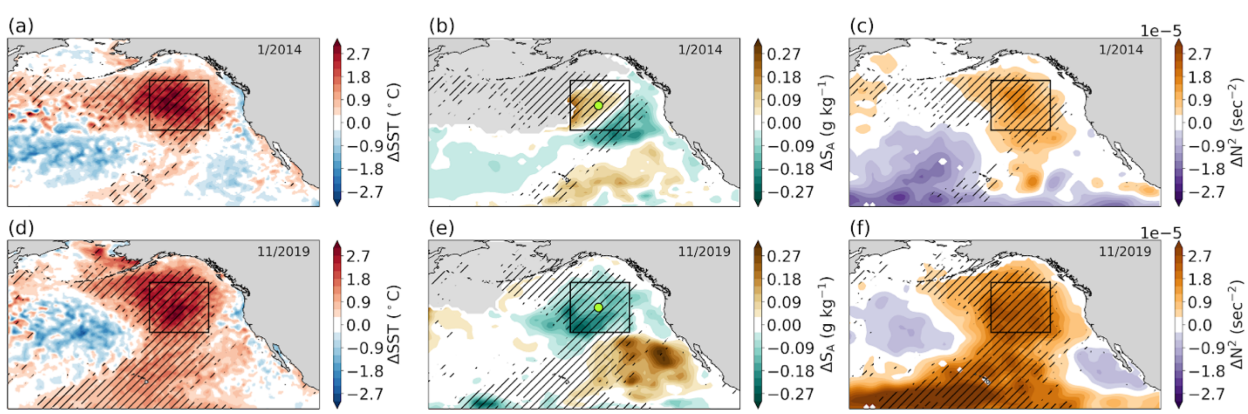

Figure 1. Spatial characteristics of NE Pacific MHWs during January 2014 (a-c) and November 2019 (d-f); the two warmest months of SST anomalies averaged in the boxed region from 2004

through 2020. First column (a,d) shows SST anomalies from the OISSTv2 where diagonal hatching indicates the locations experiencing a MHW. Hatching across columns is consistent. The middle column (b,d) is the absolute salinity anomaly on 25.4 kg m^{-3}. By definition, conservative temperature anomalies mirror salinity anomalies on isopycnals where conditions are either warm/salty or cool/fresh. The third column (c,f) shows the bulk upper ocean stability anomaly in terms of the Brunt-Väisälä frequency squared computed using the anomalous density difference between 2.5 and 200 dbar. All anomalies are referenced to the January 2004 through June 2020 monthly climatology. The bounding black box represents the area defined by 35.5–51.5°N, 135.5–154.5°W and the lime green circles in (b) and (c) mark 43.5°N, 145.5°W. Gray shading in panels b, c, e, and f (excluding land) shows the locations where 25.4 kg m^{-3} outcrops in January 2014 (b,c) and November 2019 (e,f).

Positive stratification (N^2) anomalies occurred for both the 2013–2016 and 2019–2020 MHWs, however they were much greater in 2019 (Figure 1, Movie S1). Warm and fresh near-surface anomalies in 2019 decreased density and increased the stratification (Figure 2), whereas in 2013–2016 the near-surface density reduction from a warm anomaly was partially offset by a salty anomaly. The increase in pressure along 25.4 kg m^{-3} beginning in 2018 reflects an increase in stratification even before the onset of the 2019 MHW (Figure 2). The 2019 large and positive stratification anomaly likely inhibited the surface MHW from penetrating as deeply as the 2013–2016 MHW, and furthermore may have enhanced the surface build-up of heat.

Prior to 2013, two other noteworthy MHWs occurred in the NE Pacific from 2004–2005 and 2008–2009 (Figure 2). Warm subsurface Θ anomalies during these MHWs extended and propagated to depths beyond 100 dbar and anomalies at 25.4 kg m^{-3} were spicy, similar to that of the 2013–2016 event (Figure 2). Warm and salty anomalies reduced subsurface density and increased the stratification of the surface layer. The 2004–2005 MHW was more stratified than the 2008-2009 event owing to the larger surface density anomaly (Figure 2e and Figure 5b-c).

The simultaneous change in temperature from 0–200 dbar in 2008–2009 could have resulted from isopycnal heave, as indicated by the downward deflection of 26.3 kg m^{-3} (Figure 2a). Heave can occur in response to Ekman pumping due to wind stress curl that depresses the main thermocline (Bindoff and McDougall, 1994), or from other dynamic features such as large-scale Rossby waves (Xie et al., 2016) or eddies (Pegliasco et al., 2015). Positive pressure anomalies on 26 kg m^{-3} indicates a deepening of the thermocline in 2008–2009 at approximately 130 dbar (Figure 2f). These vertical isopycnal motions are nearly adiabatic. As seen from the conservation of water mass properties on the isopycnal (Figure 2b,d), there is little exchange of heat or salinity with the surrounding environment. As a result, warm and fresh anomalies in 2008–2009 occurred along the 150–200 isobars, however, were negligible on 26.3 kg m^{-3}, which ranges from 150–200 dbar (Figure 2).

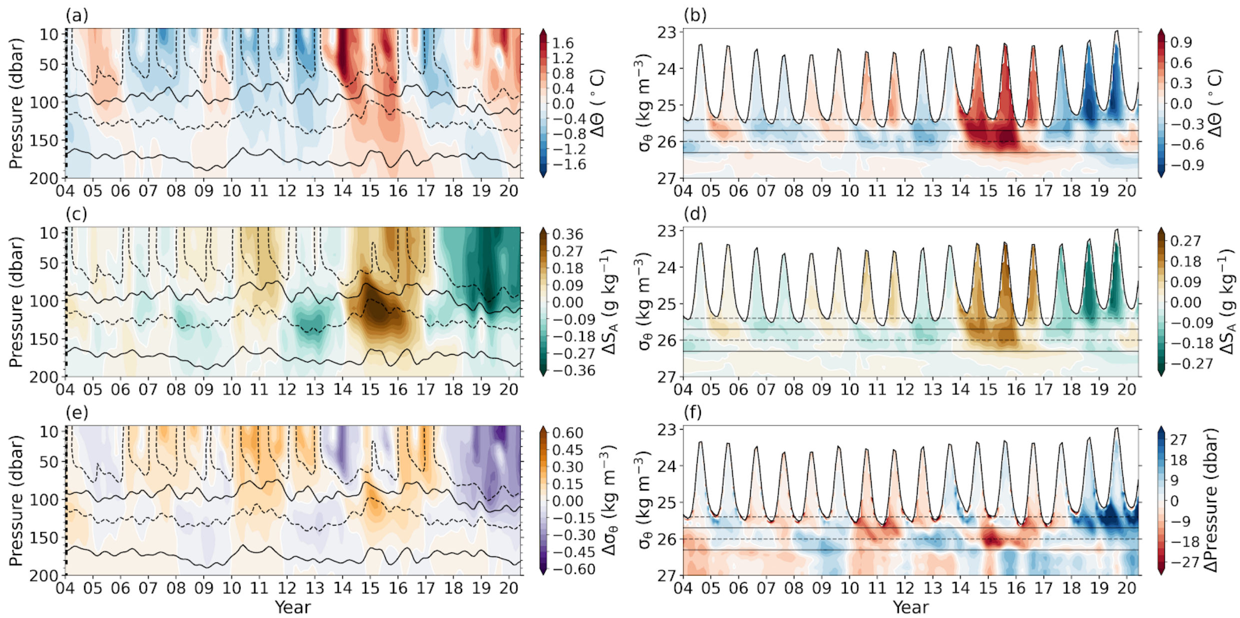

Figure 2. Progression of monthly anomalies in (a,b) conservative temperature, (c,d) absolute salinity, (e) potential density, and (f) isopycnal pressures at 43.5°N, 145.5°W (lime green circles in Figure 1) from January 2004 through June 2020. Contours of the 25.4 kg m^{-3} (upper dashed), 25.7 kg m^{-3} (upper solid), 26 kg m^{-3} (lower dashed), and 26.3 kg m^{-3} (lower solid) isopycnal surfaces vary with pressure (a,c,e), however are constant when plotted against density (b,d,f).

Analysis of $\Theta - S_A$ relationships along isopycnals provides additional insight into water-mass property changes during MHWs. Here, spice is primarily controlled by the exchange of heat and freshwater between the ocean and atmosphere, ocean turbulent mixing, and lateral advection. Spicy conditions occurred each winter (December-January-February) during the 2013–2016 MHW, most notably in waters lighter than 26.5 kg m^{-3} during the winters of 2014/15 and

2015/16 (Figure 3a). The warmest wintertime temperatures occurred in 2013/14 where $\Theta - S_A$ variations were confined to lighter isopycnals (<26 kg m^{-3}). Winter spice anomalies in 2013/14 likely mixed to denser isopycnals in the permanent halocline by summer, as can be seen along 25.6 kg m^{-3} during the summers of 2014 and 2015 (Figure 3b). By summer 2016, spice anomalies within the permanent halocline returned to near normal, however the seasonal thermocline remained anomalously warm and salty. Spice anomalies during the summer 2019 MHW were minty compared to average. Minty conditions in June-July-August of 2019 were greatest within the seasonal thermocline above 25.5 kg m^{-3} (Figure 3b). As a consequence, the near surface $\Theta - S_A$ properties were much lighter compared to 2014–2016, both in winter and summer seasons. Minty conditions persisted into the winter of 2019/20.

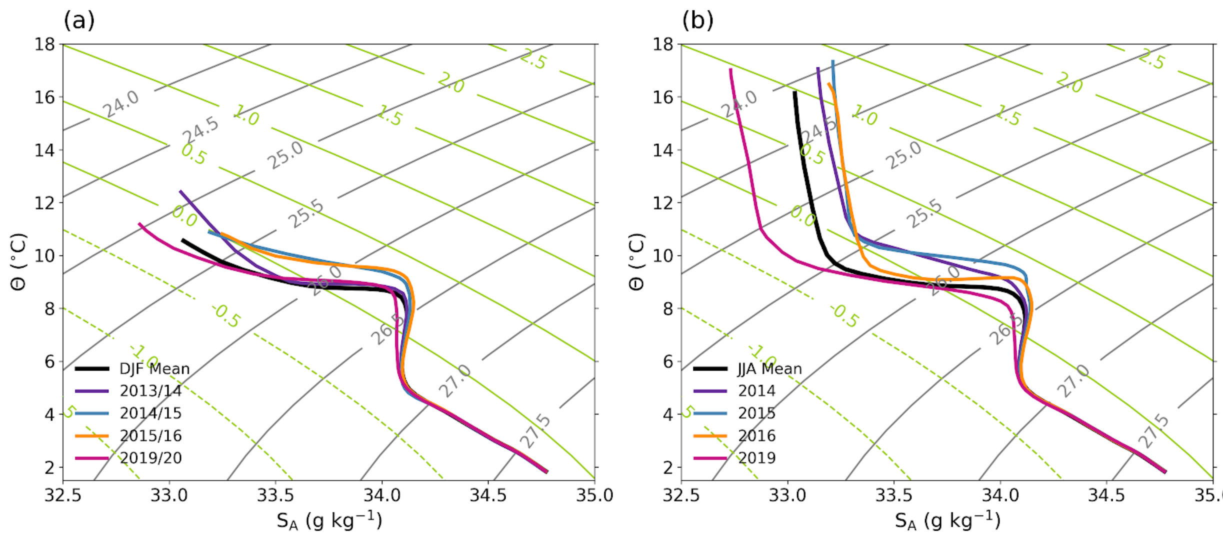

Figure 3. Winter (December-January-February) (a) and summer (June-July-August) (b) temperature-salinity relationships at 43.5°N, 145.5°W (lime green circles in **Figure 1**). The average 2004–2019 DJF and 2004–2019 JJA curves are shown by the thick black lines. Contours of constant spice (kg m^{-3}) in green are perpendicular to isopycnals in gray.

A connection between the evolution of surface and subsurface anomalies was a recurring theme during recent 2013–2016 and 2019–2020 NE Pacific MHWs and is visible in both Figures 2 and 4. To quantify the time lags associated with the penetrations of surface anomalies into the subsurface, we compute the lagged cross-correlation for Θ and S_A on isobars and isopycnals with values at 2.5 dbar and 25.7 kg m^{-3} respectively. Significant positive correlations between surface and subsurface $\Theta - S_A$ anomalies increase with positive lag and density between 25.7–27 kg m^{-3}. For example, the maximum cross-correlation on 26.3 kg m^{-3} occurs at 6 months positive lag (Figure S3). On the other hand, subsurface anomalies (between 150–220 dbar) are most strongly correlated with the surface conditions for positive lags of 1–2 years, while subsurface SA correlations peak at 6–12 months positive lags (Figure S3 and Figure S4).

The downward progression of surface Θ and S_A anomalies suggest that the North Pacific Ocean is capable of maintaining long-term memory of surface MHWs. One measure of memory is the heat content anomaly, Q', evaluated here over equal thickness subsurface layers. The largest Q' values occur within the seasonally varying mixed layer (10–90 dbar) where temperature fluctuations are the strongest (Figure 4). The largest positive anomalies are present during the 2013–2016 MHW. After a period of strong cooling, Q' steadily increased beginning in 2018 through present. Prior to 2013 there were two smaller MHWs that occurred in 2004–2005 and 2008–2009 that also had small gains of heat content. Evaluating Q' over layers spanning the pycnocline (100–180 dbar) and interior (200–280 dbar) reveals the persistence of Θ anomalies below the surface temperature variability. Once $\Theta - S_A$ anomalies get into the subsurface, their properties are nearly conserved even after the surface cools (Figure 4).

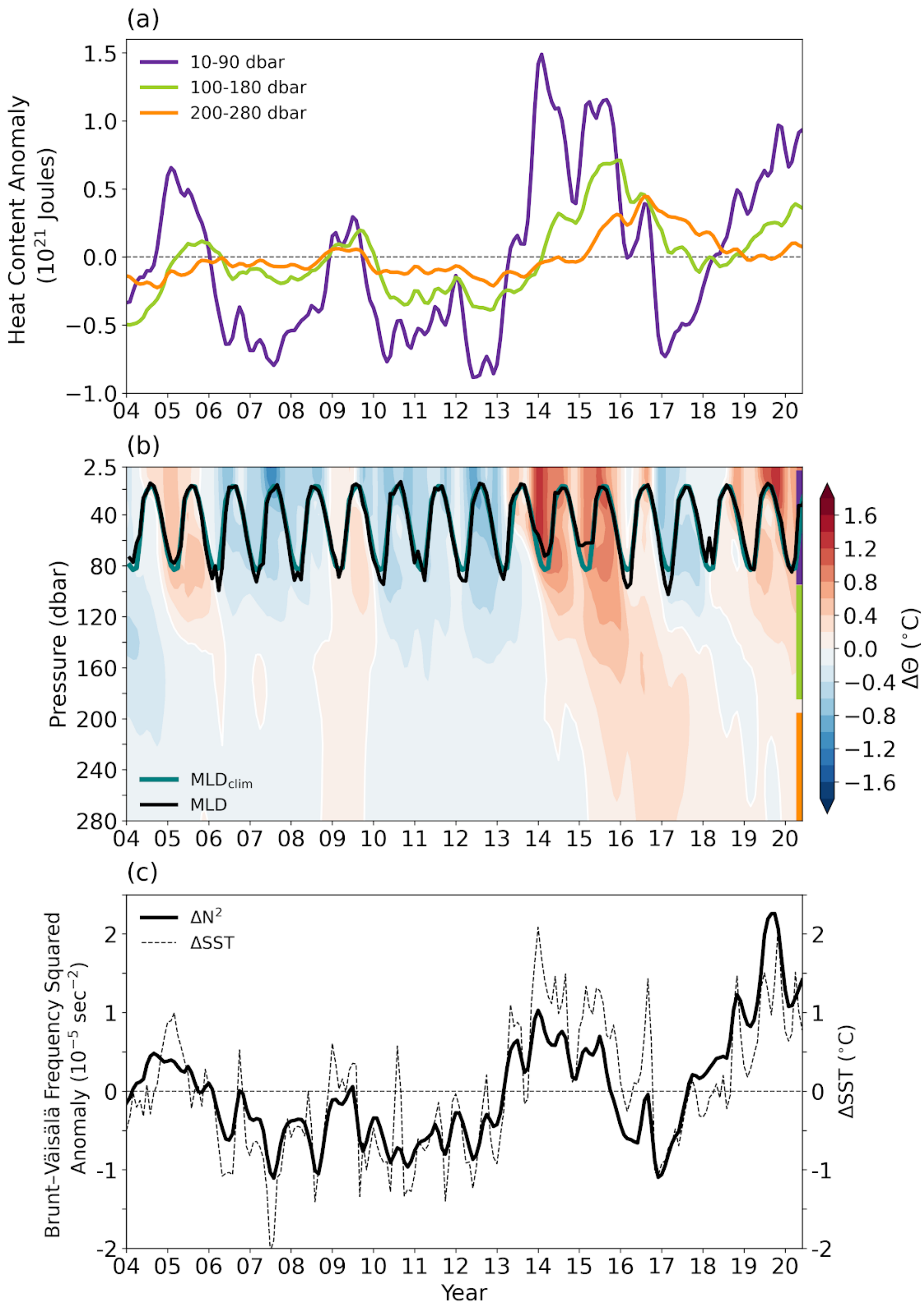

(a)
Heat Content Anomaly (10^{21} Joules)
10-90 dbar
100-180 dbar
200-280 dbar
1.5
1.0
0.5
0.0
−0.5
−1.0
04 05 06 07 08 09 10 11 12 13 14 15 16 17 18 19 20
(b)
Pressure (dbar)
2.5
40
80
120
160
200
240
280
MLD_{clim}
MLD
04 05 06 07 08 09 10 11 12 13 14 15 16 17 18 19 20
ΔΘ (°C)
1.6
1.2
0.8
0.4
0.0
−0.4
−0.8
−1.2
−1.6
(c)
Brunt-Väisälä Frequency Squared Anomaly (10^{-5} sec^{-2})
ΔN^2
ΔSST
2
1
0
-1
-2
ΔSST (°C)
04 05 06 07 08 09 10 11 12 13 14 15 16 17 18 19 20
Year

299

Figure 4. Variations in (a) upper ocean heat content anomalies, (b) temperature anomalies and mixed layer pressure, and (c) upper ocean stratification anomalies averaged in 35.5–51.5°N, 135.5–154.5°W (black outline in Figure 1). Ocean heat content anomalies are computed over three different 80-dbar pressure layers between 10–90 dbar, 100–180 dbar, and 200–280 dbar. These intervals are shown in (b) as vertical colored lines on the right-hand side corresponding to (a). The mixed layer pressure and 2004-2019 climatology is computed from 19,697 Argo profiles using the Holt and Talley (2009) density algorithm. The bulk upper ocean stratification anomaly (solid lines) in (c) is computed as N^2 between 2.5 and 200 dbar and shown with the SST anomaly (dashed lines). Positive values of N^2 indicate higher water column stability and greater resistance to overturning or vertical displacement.

An increase in upper ocean heat content can affect the stability of the upper ocean. The depth of the mixed layer also shoals, which can be seen during the winters of 2013/2014 and 2014/2015 (Figure 4). The increase in stratification reduces entrainment of cool water from below and can exacerbate warming by reducing the thickness of the surface layer that accepts heat from the atmosphere, making the surface ocean easier to warm. The upper ocean stratification anomaly was noticeably higher (large N^2 anomaly values) in 2014–2015, with the largest values occurring in 2019 (Figure 4c). The very high values in 2019–2020 arise from the anomalously fresh near-surface conditions during that MHW.

5 Discussion

This study examines 21$^{\mathrm{st}}$ Century MHWs in the NE Pacific based on gridded SST data, and also the evolution of subsurface $\Theta - \mathrm{S_A}$ anomalies from Argo on both isobars and isopycnals during the 2013–2016 and 2019–2020 NE Pacific MHWs. Upper ocean salinity was anomalously fresh in the Gulf of Alaska during the 2019–2020 MHW, which greatly increased the buoyancy of the surface layer. Indeed, there was a net freshwater input from precipitation as can be seen in the 2018 precipitation anomaly in the Gulf of Alaska (Yu et al., 2019) that likely contributed to the decrease in surface salinity (Reagan et al., 2019). The resulting increase in stratification during 2019–2020 likely contributed to the decrease in the depth (and density) to which water property anomalies from this event were detrained, and in places subducted. The confinement of warm anomalies to the near-surface likely enhanced the MHW’s intensity.

There are several dynamical pathways by which surface MHW anomalies in the NE Pacific could reach the subsurface; by means of detrainment, diabatic subduction (Jackson et al., 2018), lateral advection (Chao et al., 2017; Zaba et al., 2020), and/or adiabatic isopycnal heave. Subduction occurs in subtropical regions after temperature anomalies within the deep wintertime mixed layer detrain as a result of the mixed layer retreating in late spring. During the 2014 and 2015 spring transition of the mixed layer depth, subsurface warming occurred along both isopycnals and isobars below the mixed layer, suggesting that diabatic vertical or horizontal mixing could play a role in the penetration of MHW anomalies within the seasonal pycnocline. Indeed, Zaba et al. (2020) attribute positive subsurface heat content anomalies within the California Undercurrent to an increase in poleward heat transport from the tropics in September 2015. Alternatively, subsurface warming that occurs primarily on isobars and not on isopycnals was likely the result of isopycnal heave, defined as the downward deflection of a potential density surface. We speculate that heave is most likely responsible for the near-simultaneous appearance of anomalies below 150 dbar, for example during the 2008–2009 MHW, however the exact mechanisms of heave (i.e., from Ekman pumping due to wind stress curl) are not investigated here.

Once surface MHW anomalies are detrained out of the deep wintertime mixed layer, they may propagate downward. The lag associated with the vertical propagation of surface anomalies causes the subsurface heat content to remain anomalously high even after surface conditions return to normal. This persistence of subsurface heat and the possible seasonal reemergence of surface anomalies could in fact help supercharge the occurrence of multi-year events. As future warming trends favor a more stratified upper ocean (Li et al., 2020), we expect that detrainment out of the mixed layer may become less effective in storing MHW anomalies in the subsurface, and therefore further amplify surface warming. This possibility is concerning owing to the impacts that accumulated heat stress and stratification have on pelagic marine ecosystems and primary production (Cavole et al., 2016; Jacox et al., 2016; Smale et al, 2019).

Mixed layer heat budgets are frequently used to diagnose the drivers of surface warming associated with MHWs; however, the influence of salinity and subsurface water mass properties are often overlooked (Holbrook et al., 2020). Using the global Argo array data, this study motivates complementary analyses on the role of salinity and subsurface $\Theta - S_A$ anomalies to better understand the ocean's role in the persistence and evolution of long-lived events. Further investigation into the drivers of salinity anomalies and their role in the development of NE Pacific MHWs would appear to be a fruitful avenue of future research. Analysis of the full 4-D heat budget using high resolution numerical models could be undertaken to investigate the local mechanisms of subsurface warming.

Acknowledgments and Data Availability

HAS and LT are supported by an AI for Earth Innovation Grant sponsored by the Leonardo DiCaprio Foundation and Microsoft, and wish to acknowledge cloud resources from an Azure compute grant awarded through Microsoft's AI for Earth. GCJ and JML are supported by NOAA Research and NOAA's Global Ocean Monitoring and Observing Program. HAS and SCR were also partially supported by NOAA via grant NA15OAR4320063 to the University of Washington through the Joint Institute for the Study of the Atmosphere and Ocean. This is PMEL Contribution Number 5140. The NOAA OISSTv2 dataset was provided by the NOAA/OAR/ESRL PSL, Boulder, Colorado, USA, from their Web site at https://psl.noaa.gov/. Argo data were collected and made freely available by the International Argo Program and the national programs that contribute to it (http://www.argo.ucsd.edu and http://argo.jcommops.org). The Argo Program is part of the Global Ocean Observing System. Lastly, we would like to thank two anonymous reviewers whose comments helped to improve this manuscript.

References

Alexander, M. A., & Deser, C. (1995), A Mechanism for the Recurrence of Wintertime Midlatitude SST Anomalies. *Journal of Physical Oceanography*, 25, 122–137, https://doi.org/10.1175/1520-0485(1995)025<0122:AMFTRO>2.0.CO;2

Alexander, M. A., Deser, C., & Timlin, M. S. (1999), The Reemergence of SST Anomalies in the North Pacific Ocean. *Journal of Climate*, 12, 2419–2433, https://doi.org/10.1175/1520-0442(1999)012<2419:TROSAI>2.0.CO;2

Alexander, M. A., Timlin, M. S., & Scott, J. D. (2001), Winter-to-winter recurrence of sea surface temperature, salinity and mixed layer depth anomalies, *Progress in Oceanography*, 49, 41-6, https://doi.org/10.1016/S0079-6611(01)00015-5

Amaya, D. J., A. J. Miller, S. Xie, & Kosaka, Y. (2020), Physical drivers of the summer 2019 North Pacific marine heatwave. *Nature Communications*, 11, 1903. https://doi.org/10.1038/s41467-020-15820-w

Bindoff, N. L., & McDougall, T. J. (1994), Diagnosing Climate Change and Ocean Ventilation Using Hydrographic Data, *Journal of Physical Oceanography*, 24, 1137-1152, https://doi.org/10.1175/1520-0485(1994)024<1137:DCCAOV>2.0.CO;2

Bond, N. A., Cronin, M. F., Freeland, H., & Mantua, N. (2015), Causes and impacts of the 2014 warm anomaly in the NE Pacific. *Geophysical Research Letters*, 42(9), 3414-3420. https://doi.org/10.1002/2015GL063306

Cavole, L. M., Demko, A. M., Diner, R. E., Giddings, A., Koester, I., Pagniello, C. M. L. S., Paulsen, M. -L., Ramirez-Valdez, A., Schwenck, S. M., Yen, N. K., Zill, M. E., & Franks, P. J. S. (2016), Biological impacts of the 2013–2015 warm-water anomaly in the Northeast Pacific: Winners, losers, and the future. *Oceanography*, 29(2), 273–285, https://doi.org/10.5670/oceanog.2016.32

Chao, Y., Farrara, J. D., Bjorkstedt, E., Chai, F., Chavez, F., Rudnick, D. L., Enright, W., Fisher, J. L., Peterson, W. T., Welch, G. F., Davis, C. O., Dugdale, R. C., Wilkerson, F. P., Zhang, H., Zhang, Y., & Ateljevich, E. (2017), The origins of the anomalous warming in the California coastal ocean and San Francisco Bay during 2014–2016, *Journal of Geophysical Research Oceans*, 122, 7537– 7557, https://doi.org/10.1002/2017JC013120.

Di Lorenzo, E., & Mantua, N. (2016), Multi-year persistence of the 2014/15 North Pacific marine heatwave. *Nature Climate Change*, 6, 1042-1047. https://doi.org/10.1038/nclimate3082

Fewings, M. R. & Brown, K. S. (2019), Regional Structure in the Marine Heat Wave ofSummer 2015 Off the Western United States. *Frontiers in Marine Science*, 6, 564. https://doi.org/10.3389/fmars.2019.00564

Gentemann, C. L., Fewings, M. R. & García-Reyes, M. (2017), Satellite sea surface temperatures along the West Coast of the United States during the 2014–2016 northeast Pacific marine heat wave. *Geophysical Research Letters*, 44, 312– 319, https://doi.org/ https://doi.org/10.1002/2016GL071039

Hobday, A. J., Alexander, L. V., Perkins, S. E., Smale, D. A., Straub, S. C., Oliver, E. C. J., Benthuysen, J. A., Burrows, M. T., Donat, M. G., Feng, M., Holbrook, N. J., Moore, P. J., Scannell, H. A., Sen Gupta, A., & Wernberg, T. (2016), A hierarchical approach to defining marine heatwaves. *Progress in Oceanography*, 141, 227-238. https://doi.org/10.1016/j.pocean.2015.12.014

Holbrook, N. J., Scannell, H. A., Sen Gupta, A, Benthuysen, J. A., Feng, M., Oliver, E. C. J., Alexander, L. V., Burrows, M. T., Donat, M. G., Hobday, A. J., Moore, P. J., Perkins-Kirkpatrick, S. E., Smale, D. A., Straub, S. C., & Wernberg, T. (2019), A global assessment of marine heatwaves and their drivers. *Nature Communications*, 10, 2624. https://doi.org/10.1038/s41467-019-10206-z

Holbrook, N. J., Sen Gupta, A., Oliver, E. C. J., Hobday, A. J., Benthuysen, J. A., Scannell, H. A., Smale, D. A., & Wernberg, T. (2020), Keeping pace with marine heatwaves, *Nature Reviews Earth & Environment*, https://doi.org/10.1038/s43017-020-0068-4

Holte, J. & Talley, L. (2009), A New Algorithm for Finding Mixed Layer Depths with Applications to Argo Data and Subantarctic Mode Water Formation. *Journal of Atmospheric and Oceanic Technology*, 26, 1920–1939. https://doi.org/10.1175/2009JTECHO543.1

Intergovernmental Oceanographic Commission, SCOR, and IAPSO (2010), The international thermodynamic equation of seawater – 2010: Calculation and use of thermodynamic properties, Intergovernmental Oceanographic Commission, Manuals and Guides No. 56, 196 pp., UNESCO

Jackson, J. M., Johnson, G. C., Dosser, H. V., & Ross, T. (2018), Warming from recent marine heatwave lingers in deep British Columbia fjord. *Geophysical Research Letters*, 45, 9757– 9764. https://doi.org/10.1029/2018GL078971

Jacox, M. G., Hazen, E. L., Zaba, K. D., Rudnick, D. L., Edwards, C. A., Moore, A. M. & Bograd, S. J. (2016), Impacts of the 2015–2016 El Niño on the California Current System: Early assessment and comparison to past events, *Geophysical Research Letters*, 43, 7072-7080, https://doi.org/10.1002/2016GL069716

Jayne, S.R., Roemmich, D., Zilberman, N., Riser, S. C., Johnson, K. S., Johnson, G. C., & Piotrowicz, S. R. (2017), The Argo Program: Present and future. *Oceanography*, 30(2), 18–28. https://doi.org/10.5670/oceanog.2017.213

Laufkötter, C., Zscheischler, J., & Frölicher, T. L. (2020). High-impact marine heatwaves attributable to human-induced global warming, Science, 369(6511), 1621-1625. https://doi.org/10.1126/science.aba0690

Li, G., Cheng, L., Zhu, J., Trenberth, K. E., Mann, M. E., & Abraham, J. P. (2020). Increasing ocean stratification over the past half-century. *Nature Climate Change*, https://doi.org/10.1038/s41558-020-00918-2

McDougall, T. J., & Krzysik, O. A. (2015), Spiciness, *Journal of Marine Research*, 73, 141-152, https://doi.org/10.1357/002224015816665589

Munk, W., 1981: Internal waves and small-scale processes. *Evolution of Physical Oceanography*, B. A. Warren and C. Wunsch, Eds., MIT Press, 264–291

Myers, T. A., Mechoso, C. R., Cesana, G. V., DeFlorio, M. J., & Waliser, D. E. (2018), Cloud feedback key to marine heatwave off Baja California. *Geophysical Research Letters*, 45, 4345–4352, https://doi.org/10.1029/2018GL078242

Oliver, E. C. J., Donat, M. G., Burrows, M. T., Moore, P. J., Smale, D. A., Alexander, L. V., Benthuysen, J. A., Feng, M., Sen Gupta, A., Hobday, A. J., Holbrook, N. J., Perkins-Kirkpatrick, S. E., Scannell, H. A., Straub, S. C. & Wernberg, T. (2018), Longer and more frequent marine heatwaves over the past century, *Nature Communications*, 9, 1324, https://doi.org/10.1038/s41467-018-03732-9

Pegliasco, C., Chaigneau, A., & Morrow, R. (2015), Main eddy vertical structures observed in the four major Eastern Boundary Upwelling Systems, *Journal of Geophysical Research Oceans*, 120, 6008– 6033, https://doi.org/10.1002/2015JC010950

Qiu, B., & Huang, R. X. (1995), Ventilation of the North Atlantic and North Pacific: Subductions Versus Obduction, *Journal of Physical Oceanography*, 25, 2374-2390, https://doi.org/10.1175/1520-0485(1995)025<2374:VOTNAA>2.0.CO;2

Reagan, J., Boyer, T., Schmid, C., & Locarnini, R. (2019), Subsurface Salinity [in “State of the Climate in 2018”]. *Bulletin of the American Meteorological Society*, 100 (9), S79–S81, https://doi.org/10.1175/2019BAMSStateoftheClimate.1

Reynolds, R. W., Smith, T. M., Liu, C., Chelton, D. B., Casey, K. S. & Schlax, M. G. (2007), Daily High-Resolution-Blended Analyses for Sea Surface Temperature, *Journal of Climate,* 20, 5473-5496, https://doi.org/10.1175/2007JCLI1824.1

Reynolds, R. W., Rayner, N. A., Smith, T. M., Stokes, D. C. & Wang W. (2002), An improved in situ and satellite SST analysis for climate, *Journal of Climate*, 15, 1609-1625, https://doi.org/10.1175/1520-0442(2002)015<1609:AIISAS>2.0.CO;2

Roemmich, D. & Gilson, J. (2009), The 2004-2008 mean and annual cycle of temperature, salinity, and steric height in the global ocean from the Argo Program, *Progress in Oceanography*, 82, 81-100, https://doi.org/10.1016/j.pocean.2009.03.004

Schmeisser, L., Bond, N. A., Siedlecki, S.A., & Ackerman, T. P. (2019), The role of clouds and surface heat fluxes in the maintenance of the 2013–2016 Northeast Pacific marine heatwave, *Journal of Geophysical Research: Atmospheres*, 124, 10772-10783, https://doi.org/10.1029/2019JD030780

Smale, D. A., Wernberg, T., Oliver, E. C. J., Thomsen, M., Harvey, B. P., Straub, S. C., Burrows, M. T., Alexander, L. V., Benthuysen, J. A., Donat, M. G., Feng, M., Hobday, A. J., Holbrook, N. J., Perkins-Kirkpatrick, S. E., Scannell, H. A., Sen Gupta, A., Payne, B. L. & Moore, P. J. (2019), Marine heatwaves threaten global biodiversity and the provision of ecosystem services, *Nature Climate Change*, 9, 306-312, https://doi.org/10.1038/s41558-019-0412-1

Xie, L., Zheng, Q., Tian, J., Zhang, S., Feng, Y., & Yi, X. (2016), Cruise Observation of Rossby Waves with Finite Wavelengths Propagating from the Pacific to the South China Sea. *Journal of Physical Oceanography*, 46, 2897–2913, https://doi.org/10.1175/JPO-D-16-0071.1

Yu, L., Jin, X., Stackhouse, P. W., Wilber, A. C., Kato, S., Loeb, N. G., & Weller, R. A. (2019), Global ocean heat, freshwater, and momentum fluxes [in “State of the Climate in 2018”]. *Bulletin of the American Meteorological Society*, 100 (9), S81–S84, https://doi.org/10.1175/2019BAMSStateoftheClimate.1

Zaba, K. D. & Rudnick, D. L. (2016), The 2014–2015 warming anomaly in the Southern California Current System observed by underwater gliders. *Geophysical Research Letters*, 43, 1241-1248, https://doi.org/10.1002/2015GL067550

Zaba, K. D., Rudnick , D. L., Cornuelle , B. D., Gopalakrishnan , G., & Mazloff , M. R. (2020), Volume and Heat Budgets in the Coastal California Current System: Means, Annual Cycles, and

Interannual Anomalies of 2014–16. *Journal of Physical Oceanography*, 50, 1435–1453, https://doi.org/10.1175/JPO-D-19-0271.1

Geophysical Research Letters

Supporting Information for

Subsurface evolution and persistence of marine heatwaves in the Northeast Pacific

H. A. Scannell[1], G. C. Johnson[2], L. Thompson[1], J. M. Lyman[2,3], S. C. Riser[1]

[1]School of Oceanography, University of Washington, Seattle, WA.

[2]Pacific Marine Environmental Laboratory, NOAA, Seattle, WA.

[3]Joint Institute for Marine and Atmospheric Research, University of Hawaii at Manoa, Honolulu, HI.

Contents of this file

Figures S1 to S4

Additional Supporting Information (Files uploaded separately)

Captions for Movies S1 to S2

Introduction

Additional figures and animations are provided to support the primary findings of the analysis and further visualize the spatiotemporal evolution of subsurface marine heatwave anomalies. We also include the availability of Argo mixed layer depths over time in the Northeast Pacific study domain.

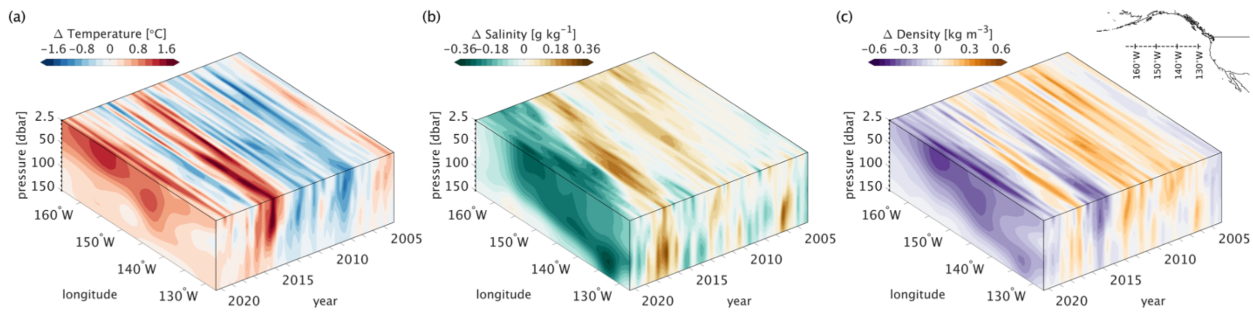

Figure S1. Subsurface evolution and vertical structure of (a) conservative temperature, (b) absolute salinity, and (c) potential density anomalies in the Northeast Pacific vs time (January 2004 through June 2020), pressure (2.5 to 150 dbar) and longitude (164.5–127.5 ºW) at 44.5 °N; see map inset. The objectively mapped Roemmich-Gilson Argo Climatology is used (Roemmich and Gilson, 2009). Anomalies are computed with respect to the January 2004 through June 2020 monthly means.

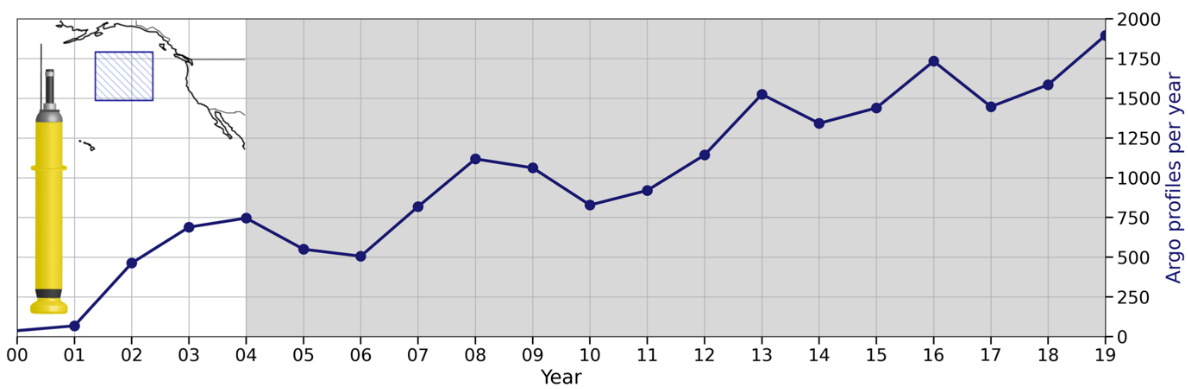

Figure S2. Number of Argo float profiles in the NE Pacific (35.5–51.5ºN, 135.5–154.5ºW; blue boxed region in map inset). Years shaded in gray are used in this analysis and overlap with the Roemmich-Gilson Argo Climatology. We use 19,697 profiles from January 2004 through June 2020. An illustration of a core Argo float is shown measuring 1.3 m in height, 20 cm wide, and approximately 40 kg in weight. These autonomous floats profile the upper 2,000 m on 10-day intervals and measure ambient seawater salinity, temperature, and pressure. The schematic of an Argo float is provided by the Argo Program (https://www.argo.ucsd.edu).

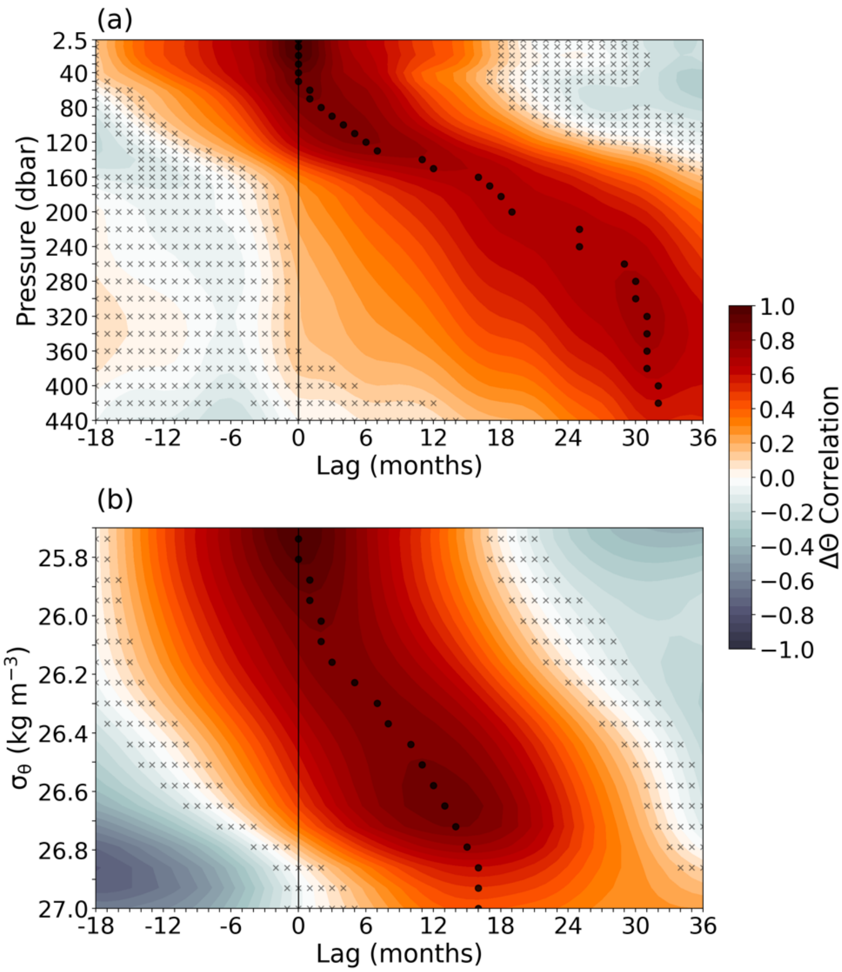

Figure S3. Lagged cross correlation between conservative temperature anomalies at (a) 2.5 dbar and (b) 25.7 kg m^{-3} with subsurface isobars (2.5–440 dbar) and isopycnals (25.7–27.0 kg m^{-3}) respectively. Anomalies are averaged within 35.5–51.5ºN, 135.5–154.5ºW (boxed outline in Figure 1). Cross correlation is computed as the Pearson's r-value ranging from -1.0 to +1.0, with larger absolute values indicating higher correlation. Cross hatching indicates insignificant correlations (p-value >= 0.05) and black circles indicate the highest positive correlation for each isobar (a) and isopycnal (b).

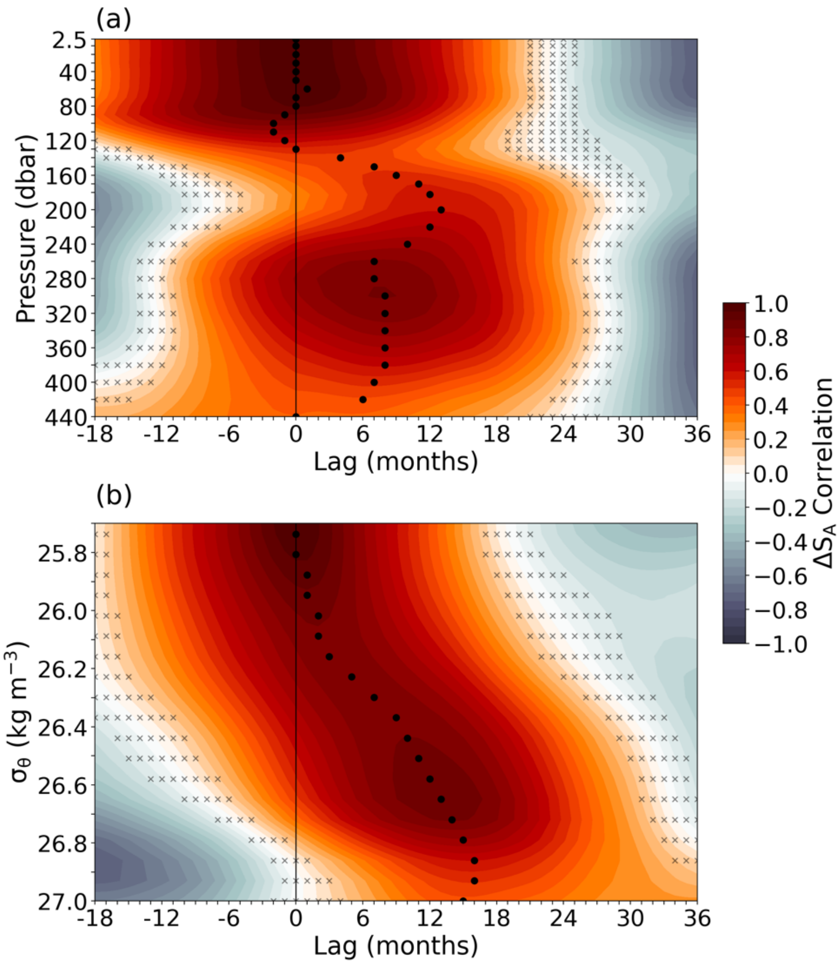

Figure S4. Lagged cross correlation between absolute salinity anomalies at (a) 2.5 dbar and (b) 25.7 kg m^{-3} with subsurface isobars (2.5–440 dbar) and isopycnal (25.7–27.0 kg m^{-3}) respectively. Anomalies are averaged within 35.5–51.5ºN, 135.5–154.5ºW (boxed outline in Figure 1). Cross correlation is computed as the Pearson's r-value ranging from -1.0 to +1.0, with larger absolute values indicating higher correlation. Cross hatching indicates insignificant correlations (p-value >= 0.05) and black circles indicate the highest positive correlation for each isobar (a) and isopycnal (b).

Movie S1. Evolution of monthly (a) sea surface temperature anomalies, (b) absolute salinity on the 25.4 kg m^{-3} isopycnal, and (c) stratification anomaly between 2.5 and 200 dbars in the Northeast Pacific marine heatwave. Contours in (c) show the pressure of the 25.4 kg m^{-3} isopycnal. Sea surface temperature anomalies are from the OISSTv2 where diagonal hatching indicates the locations experiencing a marine heatwave defined when the sea surface temperature exceeds the local monthly 90^{th} percentile averaged. Hatching over absolute salinity is consistent with (a) showing the presence of marine heatwaves in sea surface temperature. All anomalies are referenced to the January 2004 through June 2020 monthly climatology.

Movie S2. Same as in Movie S1 except on the 25.7 kg m^{-3} isopycnal.